Numerical Simulation of an Ion-Implanted GaAs OPFET

P. Chakrabarti, M. Madheswaran, A. Gupta, and N. A. Khan

***Abstract*—A numerical model of an ion-implanted GaAs optical field-effect transistor (OPFET) has been presented. The model is a physics-based one, and overcomes the major limitations of the existing models by considering both the photoconductive effect in the channel and photovoltaic effect at the gate Schottky barrier as well as the channel–substrate barrier. The exact potential profile in the channel and variation of gate depletion width and substrate depletion width in the channel as a function of position between source and drain have been computed for the first time for a nonuniformly doped channel. The model can be used to obtain the drain–current—drain–voltage characteristics, transfer characteristics, transconductance and gate-to-source capacitance of the device under dark and illuminated conditions. The model can be used as a basic tool for accurate simulation of optoelectronic integrated circuits (OEIC's) using an OPFET.**

***Index Terms*— Device simulation, GaAs MESFET, ion-implanted OPFET, photovoltaic effect, substrate photovoltage, photoconductive effect.**

I. Introduction

THE photosensitivity of the metal–semiconductor field-effect transistor (MESFET) has opened up the possibility of their use for a variety of optoelectronic applications, including high-speed optical detection, optically controlled amplification, optically controlled oscillations, optical injection locking, and optical-to-microwave conversion. The device can be incorporated in monolithic microwave integrated circuits (MMIC's) and optoelectronic integrated circuits (OEIC's) to serve as an optical-input port.

The potential of a GaAs MESFET as a high-speed low-power photodetector was first demonstrated experimentally by Baack *et al.* [1]. Later on, the optically controlled MESFET was named an optical field-effect transistor (OPFET) by Gammel *et al.* [2]. The effect of illumination on the dc and microwave characteristics of the MESFET was subsequently studied by a number of individuals [3]–[22] to have a better understanding of the various mechanisms involved, and also to explore the possible applications of the device. Some of the major works carried out and reported over the past two decades include the study of the photoresponse of the GaAs MESFET by Graffeuil *et al.* [3] and Sugeta *et al.* [4], the optical control of the GaAs MESFET by De Salles [5], and [6], microwave characteristics of the GaAs MESFET under optical direct control by Mizuno [7], optical illumination effects on the GaAs MESFET by Chaturvedi *et al.* [8], measurement of the illumination effect on static and dynamic characteristics of the GaAs MESFET for various biasing by Gautier [9], extensive measurements of the optical response of the MESFET, both at dc and microwave frequencies, by Simons [10] and Simons *et al.* [11], and large-signal characteristics of the GaAs MESFET under illumination from an He–Ne source by Darling *et al.* [12].

Closed-form analytical models for determining the dc characteristics of an ion-implanted Si MESFET under illuminated condition was developed by Singh *et al.* [13]. The model was later extended for an optically controlled GaAs MESFET by Mishra *et al.* [14]. In these models, the photoconductive effect was only considered, totally ignoring the photovoltaic effect [15]. More realistic models based on the seminumerical approach were later developed for optically controlled ion-implanted Si and GaAs MESFET's by Chakrabarti *et al.* [16], [17]. Mohammed *et al.* [18] also developed a theoretical model to determine *I–V* characteristics of a long and short channel ion-implanted GaAs MESFET under optical illumination. A model that accounts for optically generated currents in a GaAs MESFET was proposed by Madjar *et al.* [19]. The model was also validated by experimental results. The switching characteristics of an optically controlled GaAs MESFET were modeled by Chakrabarti *et al.* [20], [21] and Madjar *et al.* [22]. However, the models reported so far for ion-implanted OPFET's are based on several simplifying and restrictive assumptions.

Ion implantation is the most widely used process in the semiconductor industry for introducing controlled impurity concentration into the channels of MESFET's. From the theoretical point of view, the analysis of an optically controlled MESFET becomes complicated when the channel of the MESFET is assumed to be nonuniformly doped. This paper describes a numerical simulation method for quantitative estimation of the performance of an ion-implanted MESFET under an optically controlled condition. In this analysis, the ion-implanted profile has been approximated by a Gaussian distribution. The reason for this is that the results obtained for the Gaussian profile are quite general. Independent adjustment of parameters (the projected range R_p and straggle parameter σ_p) enables one to produce different types of profiles in the channel.

Manuscript received October 1, 1996; revised March 10, 1997. This paper was supported by the Department of Science and Technology, Government of India, under Grant SP/S2/L-15/95.

P. Chakrabarti is with Department of Electronics Engineering, Institute of Technology, Banaras Hindu University, Varanasi 221005, India.

M. Madheswaran is with the Department of Electronics and Communication Engineering, Mohamed Sathak Engineering College, Kilakarai, 623806 Tamil Nadu, India.

A. Gupta is with Hindalco, 231217 Renukoot, India.

N. A. Khan is with Birla-Horizon, 201305 Noida, India.

Publisher Item Identifier S 0018-9480(98)07254-8.

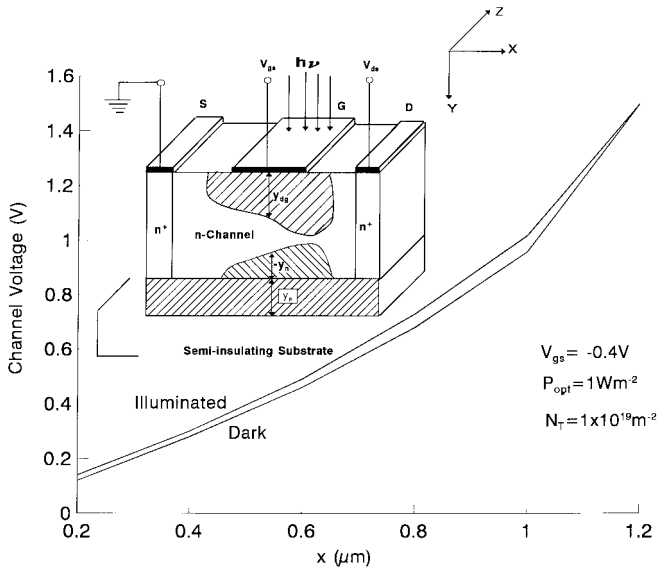

Fig. 1. Variation of the channel voltage with the distance x along the channel, together with the structure shown as an inset.

II. Theoretical Modeling

The structure under consideration is shown, as an inset, in Fig. 1. It consists of an ion-implanted n-region formed on a semi-insulating substrate. The metal gate has been assumed to be semitransparent. The drain-to-source current flows in the horizontal x-direction and the optical radiation is incident along the vertical y-direction on the semitransparent metal gate. The optical radiation is absorbed in the gate depletion region, neutral channel region, substrate depletion region, and bulk substrate region. The excess carriers cause a change in the built-in potential at the Schottky contact and channel–substrate barrier due to a photovoltaic effect, and modulates the conductivity of the channel and enhances the substrate leakage current due to the photoconductive effect.

The one-dimensional (1-D) Poission's equation in the gate depletion region in the illuminated condition with the Schottky contact as the reference can be written as

$$\frac{d^2\phi(y)}{dy^2} = -\frac{q}{\varepsilon}\left[N_d(y) + \frac{P_{\rm opt}(1-r_m)(1-r_s)\alpha\tau_L \exp(-\alpha y)}{h\nu} - \frac{R_s}{S}\right] \quad (1)$$

where $\phi(y)$ is the potential at any point y, q is the electronic charge, ε is the permittivity of the semiconductor, $P_{\rm opt}$ is the incident optical-power density (watts per square meter), r_m is the reflection coefficient at the entrance, r_s is the reflection coefficient at the metal–semiconductor contact, h is the Planck's constant, ν is the frequency of the incident radiation, α is the optical absorption coefficient of the semiconductor at the operating wavelength, τ_L is the mean lifetime of the minority carriers in the illuminated condition [17], R_s is the surface recombination rate at the metal–semiconductor interface [20], and S is the surface recombination velocity. $N_d(y)$ corresponds to the donor concentration, which can be written as a function of y in the case of an ion-implanted channel as

$$N_d(y) = \frac{D_I}{\sqrt{2\pi}\sigma_p}\exp\left[\frac{-(y-R_p)^2}{2\sigma_p^2}\right] \quad (2)$$

where R_p is the projected range, σ_p is the straggle parameter, and D_I is the ion dose of the implanted profile.

Equation (1) is subjected to the following boundary conditions:

$$\begin{aligned} \phi(0) &= V_{\rm g} - V_{\rm bil} + V_{\rm OP} \\ \phi'(y_{\rm dg}) &= 0 \\ \phi(y_{\rm dg}) &= V(x) - \Delta \end{aligned} \quad (3)$$

where ϕ' is the first derivative of potential ϕ with respect to y, $V_{\rm g}$ is the applied gate voltage, $V_{\rm bil}$ is the built-in potential of Schottky gate contact, $V_{\rm OP}$ is the photovoltage developed at the contact under illumination, $y_{\rm dg}$is the depth of the gate depletion region in the channel measured from the metal–semiconductor interface, $V(x)$ is the channel voltage at any point x due to the applied drain-to-source voltage, Δ is the depth of the Fermi level below the conduction band in the undepleted channel, and $\phi'(y_{\rm dg})$ denotes the electric field at the edge of the gate depletion region.

The 1-D Poission's equation under an illuminated condition in the space–charge region of the channel–substrate junction with the metallurgical junction taken as the reference can be written as

$$\frac{d^2\phi(y)}{dy^2} = -\frac{q}{\varepsilon}\left[N_d(a-y) + \frac{P_{\rm opt}(1-r_m)(1-r_s)\exp(-\alpha a)\alpha\tau_L}{h\nu} \cdot \exp(-\alpha|y|) - N_a\right], \quad \text{for } -y_n < y < y_p \quad (4)$$

where a is the thickness of the channel, y_n and y_p are the width of the substrate depletion regions in the channel and in the substrate bulk, respectively, and N_a is the acceptor concentration in the π-type substrate. Equation (4) is subjected to the following boundary conditions:

$$\phi(-y_n) = V(x) - \Delta, \qquad \phi'(-y_n) = 0 \quad (5)$$

$$\phi(y_p) = V_{\rm bs} + V_{\rm bi2} + V_{\rm OPS}, \qquad \phi'(y_p) = 0 \quad (6)$$

where $V_{\rm bs}$ is the substrate-to-source voltage, $V_{\rm bi2}$ is the built-in potential at the channel–substrate junction, and $V_{\rm ops}$ is the photovoltage developed across the junction in the illuminated condition.

A. Photo-Induced Voltages

Under an illuminated condition, there is a development of photovoltage ($V_{\rm OP}$) at the Schottky contact as well as at the junction between channel and substrate ($V_{\rm OPS}$) [21]. Assuming the incident radiation to decrease exponentially with the vertical distance y in the semiconductor, the total photogeneration in the gate depletion region can be obtained as

$$G_{\rm OP} = Z\frac{P_{\rm opt}}{h\nu}\alpha(1-\tau_m)(1-\tau_s)\int_0^L\int_0^{y_{\rm dg}(x)}\exp(-\alpha y)\,dy dx \quad (7)$$

where Z is the width of the gate and L is the gate length. The upper limit $y_{\rm dg}$ depends on the channel voltage and, thus, also on x.

In the presence of a large gate bias resistance, the photovoltage developed at the Schottky contact can be approximated by the open-circuit voltage, given by

$$V_{\rm OP} = \left[\frac{nkT}{q}\right]\ln\left[\frac{\frac{qG_{\rm OP}}{ZL} - R_s q}{J_{\rm sc}}\right] \tag{8}$$

where n is the ideality factor, k is the Boltzmann's constant, T is the absolute temperature, and $J_{\rm sc}$ is the reverse saturation-current density of the Schottky contact.

The photovoltage developed across the channel–substrate junction is determined by the photogenerated carriers in the substrate depletion region, as well as in the bulk substrate region (within the electron diffusion length) diffusing into the depletion region. The photogeneration in the substrate region $(G_{\rm OPS})$ has been calculated by numerically integrating (9), shown at the bottom of this page, where L_D is electron diffusion length on the substrate side. The photovoltage developed across the channel–substrate junction can be estimated from

$$V_{\rm OPS} = \left[\frac{nkT}{q}\right]\ln\left[\frac{\frac{qG_{\rm OPS}}{ZL}}{J_{\rm ssc}}\right] \tag{10}$$

where $J_{\rm ssc}$ is the reverse saturation current density at the channel–substrate junction.

B. I–V Characteristics

The drain current $I_{\rm ds}$ has been calculated by numerically integrating the charge in the channel region, given by

$$I_{\rm ds} = \frac{\mu_n Z}{L}\int_0^{V_{\rm ds}} Q_n(V)\,dV \tag{11}$$

where μ_n is the mobility of electrons, and $Q_n(V)$ is the charge in the neutral channel region per unit area at a point x where the channel voltage is $V(x)$, given by (12), shown at the bottom of this page.

In the above integrals, $y_{\rm dg}$ and y_n are functions of the channel voltage $V(x)$ and, hence, a function of the position x between source and drain.

C. Channel-Voltage Profile

In order to obtain the channel-voltage profile, the entire channel is divided into a large number of elementary strips. The differential voltage drop across the channel over the elementary distance dx along the channel at any point x is given by

$$dV = \frac{I_{\rm ds}}{q\mu_n N_{\rm av} A(x)}\,dx \tag{13}$$

where $A(x)$ is the cross-sectional area of the undepleted channel strip at x, and $N_{\rm av}$ is the average carrier density in each strip calculated numerically. The transconductance g_m and gate-to-source capacitance, $C_{\rm gs}$ of the device are given by

$$g_m = \left.\frac{dI_{\rm ds}}{dV_{\rm gs}}\right|_{V_{\rm ds}=\text{constant}} \qquad C_{\rm gs} = \left.\frac{dQ_d}{dV_{\rm gs}}\right|_{V_{\rm ds}=\text{constant}}. \tag{14}$$

D. Computational Technique

The basic model equations (1) and (4) are second-order ordinary differential equations which have been solved numerically using the Adams–Moulton method. The initial values are calculated using fourth-order Runge–Kutta method.

In order to solve a second-order differential equation of the form given by (1) and (4), the initial values of potential ϕ and its first derivative are needed. We have adopted an iterative approach to calculate these values with the help of available boundary conditions. The solution of these equations provides the values of $y_{\rm dg}$, y_n, and y_p. The variations of $y_{\rm dg}$ and y_n with the channel voltage have been calculated numerically by increasing the channel voltage in steps and repeating the computation.

In order to obtain the channel-voltage profile, we divide the channel into elementary strips and calculate the voltage drop across each strip using (13). The channel potential at the source end of the gate has been assumed to be zero. The potential at subsequent points toward the drain end separated by dx is then calculated using (13) until the drain end of the gate is reached for an assumed value of drain-to-source current. The values are used to numerically evaluate the integrals in (12) and (11) to find the drain current. The value of drain current obtained in this method is subsequently used for determining the channel-voltage profile from (13). The accurate values of $I_{\rm ds}$ and the channel-voltage profile are finally determined iteratively.

From previous computations, the variations of $y_{\rm dg}$ and y_n with channel voltage is known. The channel-voltage profile is then used to obtain the variation of the gate depletion width $y_{\rm dg}$ and the substrate depletion width y_n in the channel with the distance x. These results are used to estimate $G_{\rm OP}$, $G_{\rm OPS}$, and $Q_n(V)$ by numerically evaluating the integrals in (7), (9), and (12), respectively, which are subsequently used for the numerical evaluation of $V_{\rm OP}$, $V_{\rm OPS}$, and drain-to-source current $I_{\rm ds}$.

$$G_{\rm OPS} = \frac{P_{\rm opt}}{h\nu} Z\alpha(1-\tau_m)(1-\tau_s)\left[\int_0^L\int_{a-y_n(x)}^{a}\exp(-\alpha y)\,dydx + \int_0^L\int_a^{a+L_D}\exp(-\alpha y)\,dydx\right] \tag{9}$$

$$Q_n(V) = q\int_{y_{\rm dg}}^{a-y_n} N_d(y)\,dy + q\frac{P_{\rm opt}}{h\nu}\alpha\tau_L(1-\tau_m)(1-\tau_s)\int_0^{a-y_n}\exp(-\alpha y)\,dy \tag{12}$$

The *I–V* characteristics of the device has been obtained by the numerical integration of (11) for different values of drain-to-source voltage. The transfer characteristics of the device can be obtained by changing V_{gs} and computing the drain current for a given drain-to-source voltage by repeating the above method. The channel transconductance and gate-to-source capacitance have been numerically obtained as a function of gate voltage by using the following forms of (14):

$$g_m\{V_{\rm gs}(i)\} = \frac{I_{\rm ds}(i+1) - I_{\rm ds}(i-1)}{V_{\rm gs}(i+1) - V_{\rm gs}(i-1)} \tag{15}$$

$$C_{\rm gs}\{V_{\rm gs}(i)\} = \frac{Q_d(i+1) - Q_d(i-1)}{V_{\rm gs}(i+1) - V_{\rm gs}(i-1)} \tag{16}$$

where $I_{\rm ds}(j)$, $V_{\rm gs}(j)$, and $Q_d(j)$ denote the value of the corresponding parameters at the jth step. In order to obtain the characteristics of the device in the dark condition, the above procedure is repeated by putting $P_{\rm opt} = 0$ at appropriate places.

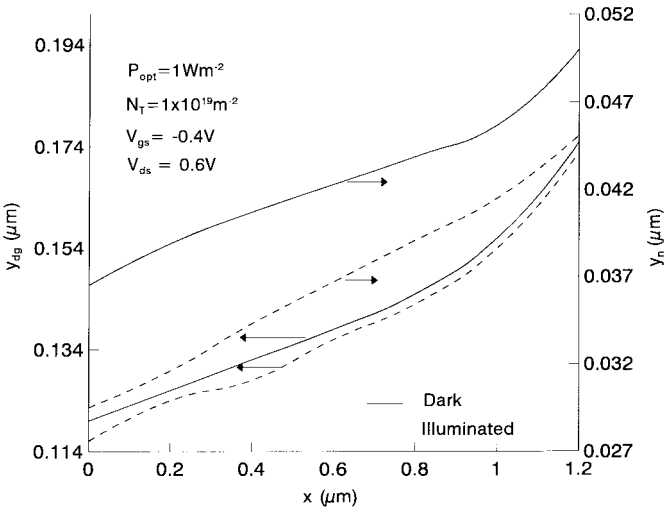

Fig. 2. Variation of the gate depletion width $y_{\rm dg}$ and substrate depletion width y_n in the channel with distance x.

III. Results and Discussion

Computations have been carried out for ion-implanted GaAs MESFET's at 300 K under dark and illuminated conditions. The gate metallization has been assumed to be thin enough to allow 90% of the incident radiation to pass through. The reflection coefficients at the metal–semiconductor interface has been calculated using [17]. The implant projected range parameter (R_p) and the straggle parameter (σ_p) are taken to be 0.20 and 0.10 μm, respectively. The implant dose (D_I) and substrate concentration (N_a) have been taken as 1.48 $\times$ $10^{16}/{\rm m}^2$ and 5 $\times$ $10^{20}/{\rm m}^3$, respectively. The absorption coefficient (α) is assumed to be 10^6/m. The gate length (L), thickness of the epi-layer, and device width (Z) have been assumed to be 1.20, 0.25, and 25 μm, respectively. Values of the parameters used in the calculation of recombination rate has been taken from [14]. The other parameters are taken from [14], [17], and [23].

Fig. 1 shows the voltage profile in the channel, which depicts the variation of the channel voltage with the distance x measured along the channel from the gate end on the source side along with the structure under consideration shown as an inset. It has been assumed that there is a negligible voltage drop between the source and gate end on the source side. Fig. 1 also shows the redistribution of the channel voltage along the x-direction in the presence of illumination (with recombination). It can be seen that while the channel voltage remains the same at the source and drain end of the gate in both dark and illuminated conditions, the channel voltages at intermediate points are more in the illuminated condition compared to those in the dark condition. Two mechanisms are responsible for the change in the channel voltage under the illuminated condition. In the presence of illumination, the conductivity of the channel increases due to the excess photogenerated carriers, which reduces the resistance of the channel. Further illumination causes a change in the conductance (through modulation of depletion depths), which results in an increase in the drain current in the illuminated condition. These two processes are competitive. However, the increase in the drain current under illuminated condition dominates the reduction in the channel resistance, resulting in an increase in the channel voltage. The reason is that the channel conductivity is decided by the majority carrier charges, which change insignificantly in the presence of illumination.

Fig. 2 shows the variation of gate depletion width and substrate depletion width in the channel with distance x along the channel under dark and illuminated conditions (with surface recombination). It is seen that the width of the gate depletion region at any point x in the channel decreases in the presence of illumination. It is interesting to note that at a given point x in the channel, the channel voltage increases in the presence of illumination (e.g., Fig. 1) while the width of the gate depletion region decreases in the presence of illumination for a given applied gate voltage. This may be accounted for by the fact that the photovoltaic effect in the illuminated condition reduces the applied gate bias and causes the net reduction in the width of the gate depletion region in the illuminated condition. Surface recombination has been found to have little effect on this variation. At a given point in the channel, the width of the substrate depletion region decreases in the presence of illumination. It is also seen that for the assumed level of illumination $(P_{\rm opt} = 1\ {\rm W/m}^2)$, the percentage change in the value of the substrate depletion width in the channel is more than the corresponding change in the gate depletion width. This is due to the large photogeneration in the substrate–channel depletion region, which is wider than the gate depletion region, and also due to the diffusion of photogenerated carriers from the substrate bulk region into the channel–substrate depletion region because of the absence of any field in the x-direction in the substrate. This makes the photovoltaic effect much more pronounced at that substrate–channel junction.

Fig. 3 shows the variations of the photovoltage developed at the Schottky contact and that at the channel–substrate junction, respectively, with the optical power density. Surface recombination has been taken into consideration in calculating the photovoltage at the Schottky contact only. It is seen that

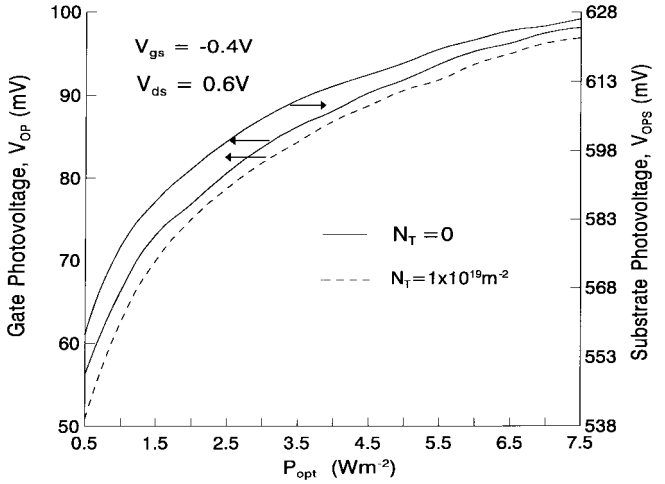

Fig. 3. Variation of the photovoltage $V_{\rm OP}$ across the Schottky barrier (with and without surface recombination) and $V_{\rm ops}$ across the channel–substrate barrier with the incident optical power density.

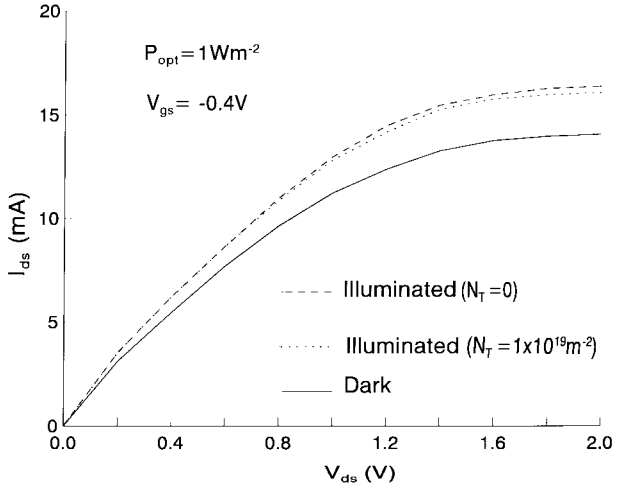

Fig. 4. Drain-to-source current $I_{\rm ds}$ versus applied drain-to-source voltage $V_{\rm ds}$ in dark and illuminated conditions.

both the photovoltage at the Schottky barrier (with and without recombination) and that at the channel–substrate barrier increase with an increase in the incident optical power density, $P_{\rm opt}$ and, finally, saturates at higher values of $P_{\rm opt}$. The saturation of these photovoltages for higher values of optical power density is due to the reduction in the lifetime of the carrier in the presence of illumination, which limits the excess photogeneration under intense illumination. It can also be seen from the Fig. 3 that the effect of surface recombination on the photovoltage developed at the Schottky barrier is dominant at lower values of $P_{\rm opt}$. This is due to the fact that for the assumed value of trap density ($N_T = 1 \times 10^{19}/{\rm m}^2$), the surface recombination becomes significant compared to photogeneration, which is low at a low optical power density. It can also be seen that for a given optical power density, the photovoltage developed at the channel–substrate barrier is much more than that developed across the Schottky barrier. This is due to a larger photogeneration in the substrate depletion region.

Fig. 4 shows the current–voltage characteristics of the device in dark and illuminated condition (with and without recombination) for an applied gate-to-source voltage of -0.4 V. It is seen that for the applied gate-to-source voltage, the drain current increases significantly in presence of illumination ($P_{\rm opt} = 1$ W/m^2). However, surface recombination tends to reduce the current in the illuminated condition. It is also seen that the saturation of the drain current in the illuminated condition takes place at a higher drain-to-source voltage (for a given $V_{\rm gs}$) than that in the dark condition. This is due to the reduction of the width of the gate and substrate depletion region in the channel in the illuminated condition, which calls for a higher drain voltage for the channel pinchoff to occur. In this model, the saturation has been assumed to be set in at a drain voltage for which the gate depletion region in the channel touches the substrate depletion region in the channel. The *I–V* characteristics obtained by the numerical method has been found to be consistent with those of the seminumerical model reported by Chakrabarti *et al.* [17].

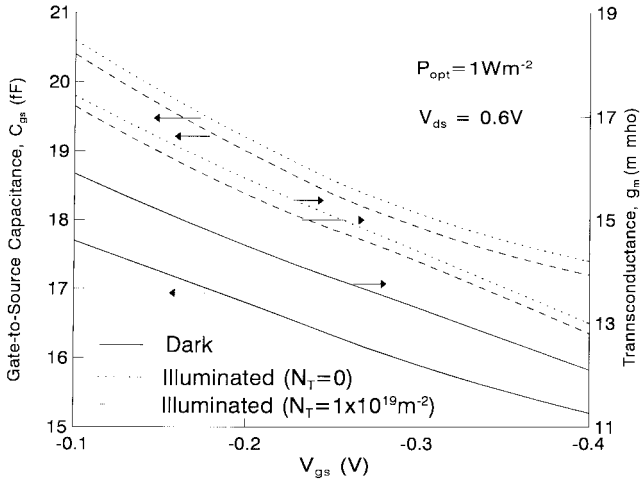

Fig. 5. Variation of transconductance g_m and gate-to-source capacitance $C_{\rm gs}$ with the applied gate-to-source voltage $V_{\rm gs}$.

Fig. 5 shows the variation of the transconductance and the gate-to-source capacitance of the device in the dark and illuminated condition (with and without recombination) with the applied gate voltage. The transconductance of the device decreases with increase in the reverse voltage for a given $V_{\rm ds}(=0.6$ V). It is also seen that the transconductance increases in the illuminated condition for a fixed $V_{\rm gs}$. This behavior is in agreement with those reported by Simons [10]. The surface recombination has a similar effect as before. The variation of the gate-to-source capacitance $(C_{\rm gs})$ of the device with gate-to-source voltage $V_{\rm gs}$ in dark and illuminated conditions (with and without recombination) reveals that $C_{\rm gs}$ decreases with an increase in $V_{\rm gs}$. However, for a particular value of $V_{\rm gs}$, the gate-to-source capacitance increases in the presence of illumination. The increase in the value of $C_{\rm gs}$ in the presence of illumination is due to the photovoltaic effect at the Schottky barrier. The assumption of a semitransparent metal gate in our case overestimates the optical effects and shows larger variations of various parameters in the illuminated condition compared to the experimentally reported results [10]. The

increase in the value of $C_{\rm gs}$ in the illuminated condition tends to increase the input *RC* time constant of the device, while the decrease in the value of g_m in the illuminated condition has an opposing effect.

IV. Conclusion

The model presented here can be used as a basic tool for simulation of OPFET's having a nonuniformly doped channel. It enables one to characterize an ion-implanted MESFET grown on a semi-insulating substrate for optically controlled applications. The numerical model developed here can be used to compute accurately the various dc characteristics of the device, including the channel-voltage profile and the variation of the gate and substrate depletion region in the channel as a function of distance between the source and drain. The model is entirely based on the physics of the device and takes into account all the major effects of illumination without making any simplifying assumptions. The model can be utilized to provide useful design guidelines for fabrication of optically controlled ion-implanted MESFET's for use in OEIC's.

References

[1] C. Bacck, G. Elze, and W. Wolf, "GaAs MESFET: A high speed optical detector," *Electron Lett.*, vol. 13, p. 193, July 1977.

[2] J. C. Gammel and J. M. Ballantyne, "The OPFET: A new high speed optical detector," in *IEEE Int. Electron Device Meeting Dig.*, Washington, DC, Dec. 1978, pp. 120–123.

[3] J. Graffeuil, P. Rossel, and H. Martinot, "Light induced effects in GaAs FET's," *Electron. Lett.*, vol. 15, pp. 439–441, July 1979.

[4] P. Sugeta and Y. Mizushima, "High speed photoresponse mechanism of GaAs MESFET," *Jpn. J. Appl. Phys.*, vol. 19, pp. L27–L29, 1980.

[5] A. A. De Salles and J. R. Forrest, "Initial observations of optical injection locking of GaAs metal semiconductor field effect transistor oscillators," *Appl. Phys. Lett.*, vol. 38, pp. 392–394, Mar. 1981.

[6] A. A. De Salles, "Optical control of GaAs MESFET," *IEEE Trans. Microwave Theory Tech.*, vol. MTT-31, pp. 812–820, Oct. 1983.

[7] H. Mizuno, "Microwave characteristics of an optically controlled GaAs MESFET," *IEEE Trans. Microwave Theory Tech.*, vol. MTT-31, pp. 596–600, July 1983.

[8] G. J. Chaturvedi, R. L. Purohit, and S. L. Sharma, "Optical effect on GaAs MESFET's," *Infrared Phys.*, vol. 23, pp. 65–68, Jan. 1983.

[9] J. L. Gautier, D. Pasquet, and P. Pouvil, "Optical effects on the static and dynamic characteristics of a GaAs MESFET," *IEEE Trans. Microwave Theory Tech.*, vol. MTT-33,pp. 819–822, Sept. 1985.

[10] R. N. Simons, "Microwave performance of an optically controlled AlGaAs/GaAs high electron mobility transistor and GaAs MESFET," *IEEE Trans. Microwave Theory Tech.*, vol. MTT-35, pp. 1444–1455, Dec. 1987.

[11] R. N. Simons and K. B. Bashin, "Analysis of optically controlled microwave/millimeter wave device structures," *IEEE Trans. Microwave Theory Tech.*, vol. 34, pp. 13349–1355, Dec. 1986.

[12] R. B. Darling and J. P. Uyemura, "Optical gain and large signal characteristics of illuminated GaAs MESFET," *IEEE J. Quantum Electron.*, vol. QE-23, pp. 1160–1171, July 1987.

[13] V. K. Singh, S. N. Chattopadhyay, and B. B. Pal, "Optically controlled characteristics of an ion-implanted silicon MESFET," *Solid State Electron.*, vol. 29, pp. 707–711, Aug. 1986.

[14] S. Mishra, V. K. Singh, and B. B. Pal, "Effect of radiation and surface recombination on the characteristics of an ion-implanted GaAs MESFET," *IEEE Trans. Electron Devices*, vol. 37, pp. 2–10, Jan. 1990.

[15] P. Chakrabarti, "Comment on effect of radiation and surface recombination of an ion-implanted GaAs MESFET," *IEEE Trans. Electron Devices*, vol. 38, p. 2578, Nov. 1991.

[16] P. Chakrabarti, R. Anand, and V. S. Rao, "*I–V* characteristics of an optically controlled Si-MESFET," *Solid State Electron.*, vol. 35, pp. 587–592, Apr. 1992.

[17] P. Chakrabarti, N. L. Shrestha, S. Srivastava, and V. Khemka, "An improved model of an ion-implanted OPFET," *IEEE Trans. Electron Devices*, vol. 39, pp. 2050–2059, Sept. 1992.

[18] S. N. Mohamed, M. S. Unlu, and H. Morkoc, "Optically controlled current voltage characteristics of an ion-implanted MESFET," *Solid State Electron.*, vol. 33, pp. 1499–1509, Dec. 1990.

[19] A. Madjar, A. Paolella and P. R. Herczfeld, "Analytical model for optically generated currents in GaAs MESFET's," *IEEE Trans. Microwave Theory Tech.*, vol. 40, pp. 1681–1691, Aug. 1992.

[20] P. Chakrabarti, S. K. Srestha, A. Srivastava, and D. Saxena, "Switching characteristics of an optically controlled GaAs MESFET," *IEEE Trans. Microwave Theory Tech.*, vol. 42, pp. 365–375, Mar. 1994.

[21] P. Chakrabarti, A. Gupta, and N. A. Khan, "An analytical model of GaAs OPFET," *Solid State Electron.*, vol. 39, pp. 1481–1490, Oct. 1996.

[22] A. Madjar, A. Paolella, and P. R. Herczfeld, "Modeling the optical switching of MESFET's considering the external and internal photovoltaic effects," *IEEE Trans. Microwave Theory Tech.*, vol. 42, pp. 62–67, Jan. 1994.

[23] S. M. Sze, *Physics of Semiconductor Devices*, 2nd ed. New York: Wiley, 1980.

P. Chakrabarti received the B.Tech. and M.Tech. degrees in radio physics and electronics from the University of Calcutta, Calcutta, India, in 1981 and 1983, respectively, and Ph.D. degree in electronics engineering from the Institute of Technology, Banaras Hindu University, Varanasi, India, in 1988.

He worked in the Department of Electrical and Electronics Engineering, Birla Institute of Technology and Science, Pilani, India, as a Faculty Member for a brief period. He joined the Department of Electronics and Communication Engineering, Birla Institute of Technology, Mesra, Ranchi, India, in 1986, as an Assistant Professor, and became an Associate Professor in 1988. He is currently working as a Professor in the Department of Electronic Engineering, Institute of Technology, Banaras Hindu University. He has also worked as Principal Investigator in many sponsored projects. Since 1984, he has been actively engaged in the research in the area of semiconductor devices in general, particularly optoelectronic devices. He has authored or co-authored over 50 research papers in international journals and has presented research papers at various international conferences in India and abroad. His current area of interest include theoretical modeling and simulation of semiconductor devices for high-speed and integrated optoelectronic applications.

Dr. Chakrabarti is a lifetime member of the Indian Society for Technical Education and the Institute of Engineers, India, and a Fellow of the Optical Society of India. He was a recipient of the Indian National Science Academy (INSA) Visiting Fellowship (1993–1994) and the Science and Engineering Research Council (SERC) Visiting Fellowship, Government of India.

M. Madheswaran was born in Salem, Tamil Nadu, India. He received the B.E. degree from Madurai Kamaraj University, in 1990, and the M.E. degree from the Birla Institute of Technology, Mesra, Ranchi, India, in 1992, both in electronics and communication engineering.

He joined the Department of Electronics and Communication Engineering, Mohamed Sathak Engineering College, Kilakarai, Tamil Nadu, India, in 1993, as a Senior Lecturer. He has also been the Branch Counselor of the IEEE student branch, Mohamed Sathak Engineering College, Kilakarai, India. From 1994 to 1997, he has been on leave, working in the Department of Electronics Engineering, Institute of Technology, Banaras Hindu University, Varanasi, India, as a Research Scholar.

Mr. Madheswaran is a life member of the Indian Society for Technical Education. He was awarded the Young Scientist Fellowship by the Tamil Nadu State Council for Science and Technology (1994–1995). He was also awarded the Senior Research Fellowship (SRF) by the Council of Scientific and Industrial Research (CSIR), Government of India.

A. Gupta received the B.E. degree in electrical and electronics engineering from Birla Institute of Technology, Mesra, Ranchi, India, in 1996.

As a part of his undergraduate summer-training program, he had worked in the area of numerical simulation of GaAs OPFET in the Department of Electronics Engineering, Institute of Technology, Banaras Hindu University, Varanasi, India. He is currently working as a Software Engineer at Hindalco, Renukoot, India.

N. A. Khan received the B.E. degree in electrical and electronics engineering from Birla Institute of Technology, Mesra, Ranchi, India, in 1996.

During his summer training program, he worked in the Department of Electronics Engineering, Institute of Technology, Banaras Hindu University, Varanasi, India, on a project related to the simulation of OPFET's. He is currently working as a Software Engineer at Birla-Horizon, Noida, India.